applied sciences

MDPI

Review

Tectonic Geodesy Synthesis and Review of the North Aegean Region, Based on the Strain Patterns of the North Aegean Sea, Strymon Basin and Thessalian Basin Case Studies

Ilias Lazos [1,*], Sotirios Sboras [2] and Christos Pikridas [3]

[1] School of Mineral Resources Engineering, Technical University of Crete, 73100 Chania, Greece
[2] Institute of Geodynamics, National Observatory of Athens, 11810 Athens, Greece; sboras@noa.gr
[3] School of Rural and Surveying Engineering, Aristotle University of Thessaloniki, 54124 Thessaloniki, Greece; cpik@topo.auth.gr
* Correspondence: ilazos@tuc.gr; Tel.: +30-2821037652

Abstract: Satellite geodesy, an indispensable modern tool for determining upper-crust deformation, can be used to assess tectonically active structures and improve our understanding of the geotectonic evolution in tectonically active regions. A region fulfilling these criteria is the North Aegean, part of the Eastern Mediterranean. It is one of the most tectonically, and hence, seismically, active regions worldwide, which makes it ideal for applying a satellite geodesy investigation. Although many regional studies have been carried out across the entire Aegean region, there are three more focused case studies that provide better resolution for different parts of the North Aegean. The synthesis of these case studies can lead to an overall geodynamic assessment of the North Aegean. The North Aegean Sea case study is characterized by the North Aegean Trough (NAT), which is directly associated with the westward prolongation of the North Anatolian Fault (NAF). Both NE–SW normal and strike-slip faulting have been documented in this offshore region. Geodetic analysis considers geodetic data, derived from 32 permanent GPS/GNSS stations (recorded for the 2008–2014 time period). This results in the estimation of the Maximum (MaHE) and Minimum (MiHE) Horizontal Extension, Maximum Shear Strain (MSS) and Area Strain (AS) parameters, based on triangular methodology implementation; the same strain parameters have similarly been estimated for the Strymon and Thessalian basins, respectively. The Strymon basin (first case study) is located in the central part of the northern Greek mainland, and it is dominated by NW–SE (up to E–W) dip-slip normal faults; this area has been monitored by 16 permanent GPS/GNSS stations for seven consecutive years. Regarding the Thessalian basin case study, E–W, dip-slip and normal faults are noted at the basin boundaries and within the Thessalian plain. This region has also been monitored for seven consecutive years by 27 permanent GPS/GNSS stations. However, this case study is characterized by a strong seismic event (Mw6.3; 3 March 2021), and thus all strain parameters depicted the pre-seismic deformation. Analysis of these three different case studies confirmed the current tectonic setting of the North Aegean region, while revealing new aspects about the geodynamic evolution of the wider region, such as highlighting areas with significant tectonic activity and the crucial role of strike-slip faulting in the broader Aegean region.

Keywords: crust deformation; GPS/GNSS analysis; North Aegean geodynamics; triangulation methodology; Greece

Citation: Lazos, I.; Sboras, S.; Pikridas, C. Tectonic Geodesy Synthesis and Review of the North Aegean Region, Based on the Strain Patterns of the North Aegean Sea, Strymon Basin and Thessalian Basin Case Studies. *Appl. Sci.* **2023**, *13*, 9943. https://doi.org/10.3390/app13179943

Academic Editor: Laramie Potts

Received: 19 June 2023
Revised: 26 August 2023
Accepted: 31 August 2023
Published: 2 September 2023

1. Introduction

Rapid technological advancements in navigation satellite missions, initially led by the US GPS (which started development in the 1970s) and subsequently other systems, such as the Russian GLONASS, Chinese Beidou and European Galileo, all integrated under the Global Navigation Satellite System (GNSS), provide an opportunity for the geoscience community to better understand plate tectonics motion and behaviour. Indeed, what was

first an approximate estimation then became a high-resolution, quantified proof of how the lithospheric plates move and deform. The first studies started in the 1990s (e.g., [1,2]), and since then, the GPS/GNSS systems have been broadly used for monitoring geodynamics in various parts of the world. In the past several years, ground station hardware and analysis techniques have also significantly improved, making the acquisition and installation of the stations more attractive economically and the data processing more precise, leading to more realistic results. In this context, the spatial resolution has improved with the denser networks, while at the same time, the time windows have also become longer, permitting more extended periods of monitoring and more accurate observations.

In the East Mediterranean, plate tectonics have created a complex geodynamic regime: the westward tectonic escape of the Anatolian microplate pushes the respective Aegean southwestwards, producing intense interplate deformation expressed by lithospheric-scale tectonic structures, and intraplate deformation, forming numerous crustal faults [3,4]. The Hellenic Subduction Zone (HSZ), also known as the Hellenic Arc, and the North Anatolian Fault Zone (NAFZ) are the dominant interplate structures associated with the intense seismic activity. The key player in Aegean geodynamics is the 80 myr evolution of the Hellenic Arc, which migrated southwards to its current position with a simultaneous roll-back of the subducting slab ([5] and references therein). This procedure left room for the Anatolian plate to push the Aegean southwestwards through the North Anatolian Fault (NAF) and its western prolongation into the North Aegean Sea, i.e., the North Aegean Trough, generating a complex seismotectonic setting along the eastern Aegean Sea—western Anatolia (Figure 1).

According to previous studies (e.g., [3,6]), the Hellenic Trench has undergone a retreat (approx. 580 km) since the Eocene–Miocene [7,8]. This geological phenomenon has resulted in a tectonic regime, which is characterized by N–S and NE–SW extensional occurrences in the Aegean and Anatolian regions [9,10]. The southwest Anatolian microplate motion is considered to be related to the exertion of pulling and pushing forces resulting from the HSZ in its western part [5]. This movement is affecting the lithospheric thickness across Anatolia and the Aegean [11,12]. The Hellenic Trench (HT) retreat results in the extensional stress field generation, causing the crustal thinning of central and northern Greece and western Anatolia ([13,14] and references therein).

In our study area (Figure 1), i.e., the northern Aegean, the North Aegean Trough (NAT) and the North Aegean Basin (NAB), two successive and interconnected tectonic structures dominate and affect a wide area of the North Aegean Sea as the western prolongation of the NAF ([15] and references therein). Specifically, these two tectonic structures cumulatively accommodate a dextral (right-lateral) motion of 24–30 mm/yr ([16] and references therein). The NAT fault zone exhibits quasi-pure shear characteristics, while the NAB region displays transtensional deformation [17]. Moreover, the smaller, less active, but evident, Central Aegean Trough (also known as the Skyros basin), which is the NAF's southern branch continuation [18–20], is the southmost transcurrent large structure in the Aegean Sea, affecting a large area bilaterally. Therefore, this area serves as a transitional zone that connects the strike-slip faulting observed along the NAF with the dip-slip, normal faulting, observed in the Greek mainland [21,22]. In particular, the NAF and its continuation divides the lithosphere, while it is considered as the northern boundary of the Aegean–Anatolian microplates ([23] and references therein). The microplates' westerly slip along this boundary, exerting pressure on the southwestern region; hence, a transtensional field is generated, which affects the surrounding area, while the formation of large basins (e.g., the Strymon and Thessalian basins) that are tectonically controlled is attributed to the same stress field [9,15,24–28]. These basins are typically delimited by antithetic (opposite displacement), normal dip-slip tectonically active faults [5,29–33]. The predominant faulting direction is E–W, which is perpendicular to the current N–S extensional field [34,35]. However, NW–SE active faults are also documented, which may reactivate previous extensional structures; these structures are related to the NE–SW, Late Miocene to Pliocene extensional phase [36,37].

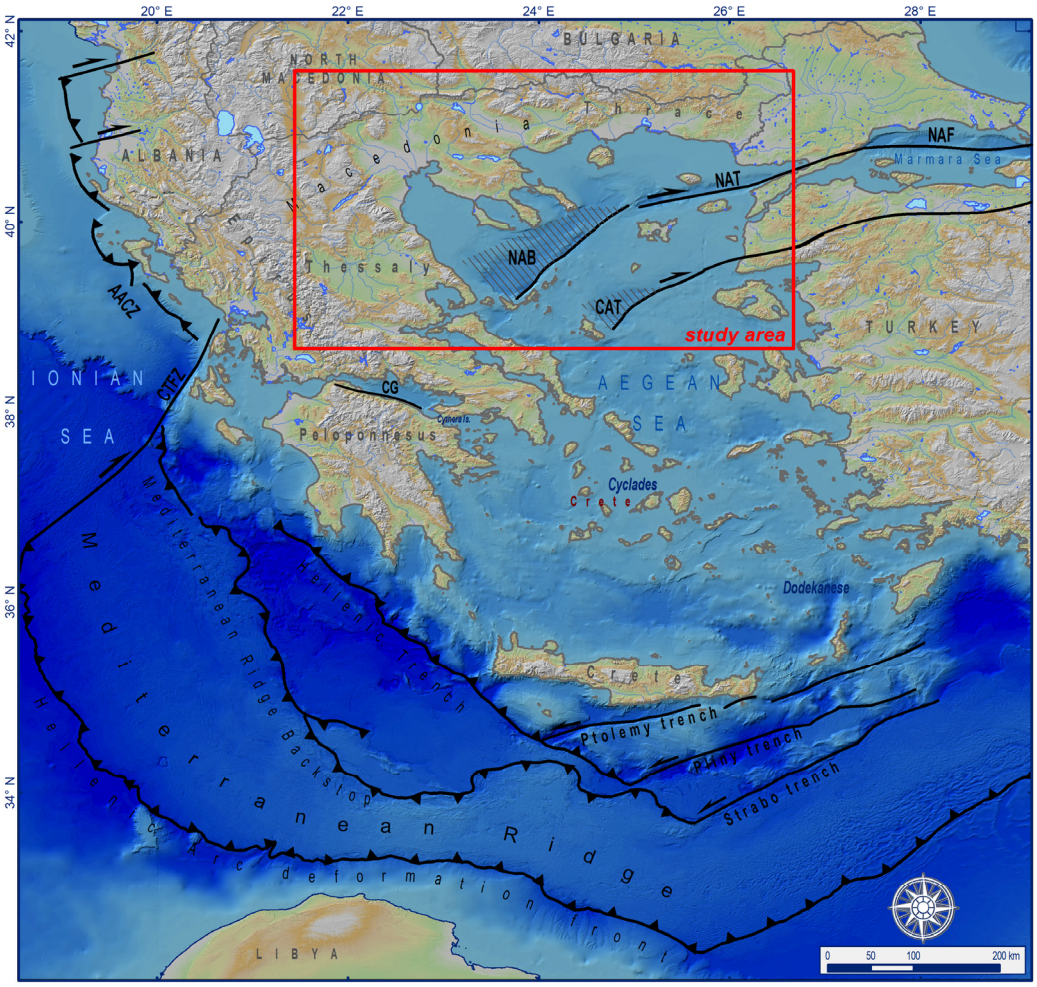

Figure 1. The main lithospheric-scale tectonic structures of the broader Aegean region (East Mediterranean). AACZ: Adria-Aegean Collision Zone, CTFZ: Cephalonia Transform Fault Zone, CAT: Central Aegean Trough, NAB: North Aegean Basin, NAF: North Anatolian Fault, NAT: North Aegean Trough, and CG: Corinth Gulf. The study area is marked by a red frame.

In such a tectonically active setting, expressed by active faults/fault zones and consequently intense seismic activity (Figure 2), monitoring of the upper-crust deformation with cutting-edge technology is crucial for recognizing and determining the behaviour of active faulting, while the contribution of field activities is considered fundamental (e.g., [38]). The aim of this paper is to provide a comprehensive synthesis and review based on geodetical results in the North Aegean region, as well as to combine and evaluate the strain parameters of three neighbouring cases studies: (i) the North Aegean Sea, (ii) the Strymon basin and (iii) the Thessalian basin. The geodetic analysis results are expected to provide qualitative and quantitative strain information, which will be used to correlate the crustal deformation with tectonically active structures.

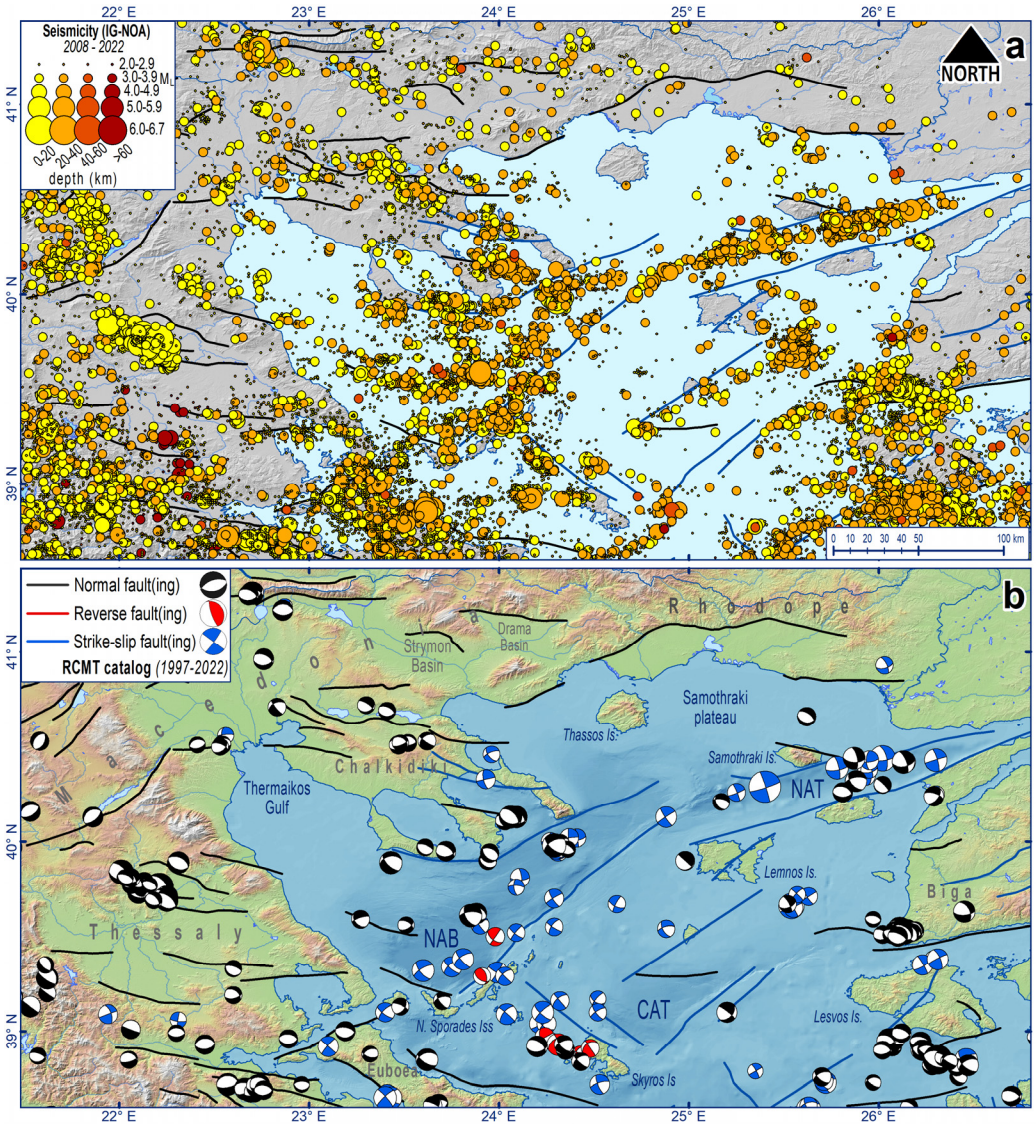

Figure 2. (**a**) Earthquake activity in the northern Aegean for a 15 yr time period (2008–2022). (**b**) Focal mechanisms from the RCMT catalogue for the period between 1997 and 2022. Beachball and fault colouring is according to kinematics. Faults in both insets are taken from GreDaSS [39,40].

2. Geodetic Studies of the Aegean Region

Since it is clear to the scientific community that satellite geodesy can provide detailed information about the motions of plate tectonics and the deformation of the crust, it is widely applied. Particularly, the Aegean and the eastern Mediterranean constitute an ideal laboratory site for geodetic analyses, and especially for the determination of strain [41–47]. Therefore, various studies have been conducted in the Aegean region by implementing measurements recorded by either permanent or campaign GPS/GNSS stations [48–53]. While preceding seismological studies only implied the gross geodynamic setting of the East Mediterranean (the relation between the Arabian, Nubian and Eurasian plates), the geodetic studies confirmed and measured plate boundaries and motions. Furthermore, they resulted in the separating of the region into several blocks, proposing potential geodynamic models (e.g., [54–57]), which are complicated. Focusing on the Aegean, two distinct velocity clusters are observed throughout the area, distributed on both sides of the NAT (and its continuation) and considered as the boundary between the North and South Aegean [58,59]. The most recent studies predominantly focus on developing crustal block modelling (e.g., [16,57,60,61]), attempting to interpret their geodynamic activity, as

well as their relationship to seismic events (e.g., [62–65]). Notably, the block modelling considers that each block partially receives the brittle tectonics effect [57,66,67], caused by tectonically active structures, while it is imprinted on the upper-crust strain. This North Aegean region strain is documented on the seismic slip and the gravitational collapse of the Aegean crustal wedge in response to slab roll-back at the Eurasian–Nubian convergence boundary [68–70], while in tandem, strike-slip faulting dominates in this region [17,23,26].

3. Materials and Methods

In this paper we exploit the strain results of three regional GPS/GNSS studies, which focus on three neighbouring areas [17,71,72]: (i) the North Aegean Sea, (ii) the Strymon basin, and (iii) the Thessalian basin. The three case studies combined can give a wider understanding of the geodynamics of the northern Aegean crustal regime. The reasons for using these results are (i) the number of the GPS/GNSS stations, (ii) the long time-period of seven years, and (iii) the consistency of the used methodology. Next, we will briefly describe the technical features and the methodological procedure, which the three case studies rely on.

Implementing permanent GPS/GNSS stations to acquire geodetic raw datasets is a dependable technique for the instrumental evaluation of deformation in the upper crust. The geodetic velocities have been predominantly employed, previously computed for Greece [73]. This paper focuses on combining the results of three study areas (North Aegean Sea, Strymon basin and Thessalian basin), which are uniformly monitored by 32, 16 and 27 GPS/GNSS stations, respectively. The stations mentioned above are incorporated within the five existing, continuously operating networks, namely HxGN/SmartNet Greece, Hepos, NoaNet, EUREF Permanent Network—EPN, and HermesNet, as documented [74]. This integration facilitates the combination of diverse datasets, thereby enabling the computation of more precise outcomes.

The abovementioned geodetic velocities were measured over seven consecutive years, specifically from 2008 to 2014 (Figure 3). Continuous 24 h region monitoring was performed over a period of seven years, with a recording interval of 30 s. It is worth noting that the GPS/GNSS data rate is 1 HZ, which is decimated to 30 s, as mentioned above. Additionally, the geodetic velocities are referenced to the European Terrestrial Reference Frame 2000 (ETRF2000), which assumes the stability of the Eurasian plate. Furthermore, it is necessary to mention that GPS/GNSS stations provide reliable information related to horizontal motions. Therefore, this paper focuses on estimating strain derived from these motions. On the contrary, the vertical displacements recorded by the GPS/GNSS stations show great errors and hence cannot be considered for the strain analysis.

The geodetic data processing considers the principles employed by European centres, wherein the Vienna Mapping Function 1 (VMF1; [75]) is executed to derive the Zenith Total Delay (ZTD) over a 2 h time interval. Furthermore, the extended analysis was conducted utilizing the IERS2003 conventions, and the geodetic raw datasets were analysed using the GAMIT/GLOBK software suite (version 10.5, Massachusetts Institute of Technology, Cambridge, MA, USA; [76,77]).

Based on all the above, the geodetic data yielded the estimation of every GPS/GNSS station's east and north velocity components and their respective errors. Several authors have widely implemented the triangulation methodology [78–83], which is regarded as the most appropriate among various methodologies (e.g., least square methodology, etc.) for processing these datasets. The fundamental theory of the triangulation methodology involves the combination of the velocity components, along with their respective errors, taken each time from three different GPS/GNSS stations, which form the vertices of a triangle; at the barycentre (centroid) of each triangle, the overall velocity is calculated and the deformation processing starts, resulting in the strain parameters estimation [17,72,84].

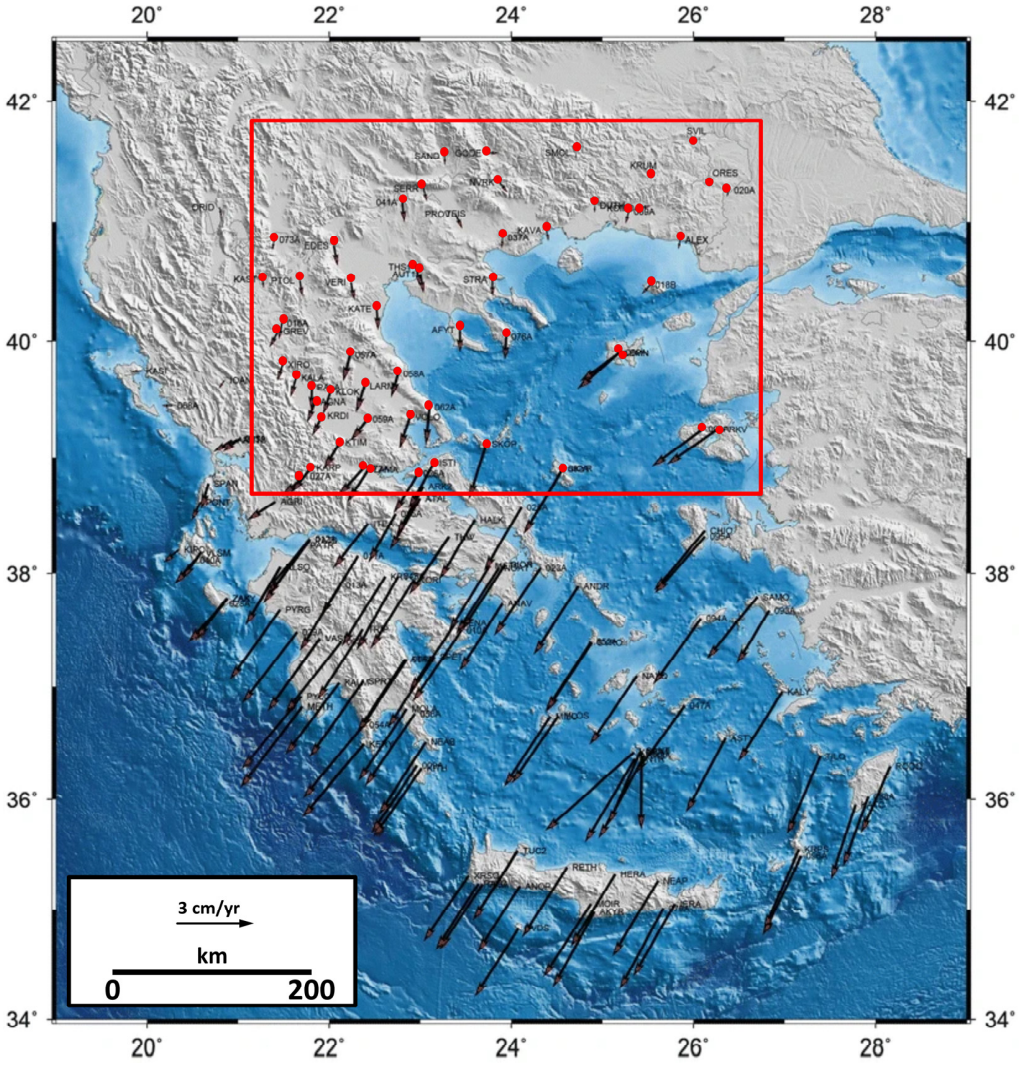

Figure 3. The GPS/GNSS stations (red dots in the red box) and the corresponding velocities (black vectors) considered for the strain analysis (modified from Bitharis et al. [73]).

A total of 404 triangles with their respective centroids were constructed for the North Aegean Sea, 216 for the Strymon basin, and 193 for the Thessalian basin, respectively. The strain parameters for each centroid were estimated using the 'GPS triangular calculator' software (UNAVCO, Boulder, CO, USA; [85]). The Maximum and Minimum Horizontal Extension (MaHE and MiHE, respectively), the Maximum Shear Strain (MaxSS) and the Area Strain (AS) are the calculated strain parameters, which will be described shortly.

However, some common characteristics of the strain parameters at this point are worth noting. In particular, all strain parameters are dimensionless; therefore, no SI units correspond to them. Nevertheless, the "nano-strain unit" has been established in the geodetically based upper-crust analysis to provide a more comprehensible expression of strain parameters. Moreover, the calculation of all parameters refers to an annual interval.

Regarding the errors of the estimated parameters, the statistical analysis of the 404 triangles revealed a range between 2% and 4% (MaHE and MiHE: 3%, MaxSS: 4% and AS: 2%). Despite the occurrence of these errors, no uncertainty is imprinted on the extracted results and therefore the geodynamic and tectonic interpretations are not affected by them.

3.1. Maximum (MaHE) and Minimum (MiHE) Horizontal Extension

The fault activity and its kinematics are strongly linked to these parameters. The Maximum Horizontal Extension (MaHE) parameter denotes instances of extensional tectonics

(extension, according to the strain nomenclature). In contrast, the Minimum Horizontal Extension (MiHE) parameter, which is perpendicular to the MaHE, denotes instances of compressional tectonics (compression, according to the strain nomenclature). Equal magnitudes of both (dilatation and compaction) reveal shear, related to strike-slip motion.

It is mentioned that the MaHE development occurrence characterizes the main axis of the strain ellipse, while the minor axis is characterized by the MiHE development, respectively. The MaHE and MiHE parameters are theoretically defined by the following equations (Equations (1) and (2)):

$$\mathrm{MaHE} = (l_f - l_0)/l_0 \quad (1)$$

$$\mathrm{MiHE} = (l'_f - l'_0)/l'_0 \quad (2)$$

where

l_f is the final length along the strain ellipse major axis,
l_0 is the original length along the strain ellipse major axis,
l'_f is the final length along the strain ellipse minor axis, and
l'_0 is the original length along the strain ellipse minor axis.

3.2. Maximum Shear Strain (MaxSS)

The Maximum Shear Strain (MaxSS) highlights areas where shear prevails and, therefore, it can be used to recognise strike-slip faults. The mathematical formulation of MaxSS is given by the following equation (Equation (3)):

$$\mathrm{MaxSS} = \mathrm{MaHE} - \mathrm{MiHE} \quad (3)$$

3.3. Area Strain (AS)

The Area Strain (AS) is a critical parameter for determining the type of crustal deformation, with two primary types being identified: (i) dilatation and (ii) compaction. Dilatation is a phenomenon that is associated with extensional active tectonics and is characterized by positive AS values. It is typically observed in regions where normal, dip-slip, or transtensional strike-slip faulting is prevalent. Conversely, compaction is indicated by the negative AS values and it is associated with compressional active tectonics where folding and thrusting prevail. The AS parameter can be represented mathematically by the following equation (Equation (4)):

$$\mathrm{AS} = \mathrm{MaHE} + \mathrm{MiHE} \quad (4)$$

4. Results

4.1. Synthesis of Strain Results

4.1.1. Maximum (MaHE) and Minimum (MiHE) Horizontal Extension

The MaHE and MiHE for the North Aegean Sea region are characterized by a wide range of strain field values. In particular, these parameters demonstrate a heterogeneous strain distribution within the North Aegean Sea region, as depicted in Figure 4a. The MaHE values range from approximately −50 to 1000 nano-strain, with the highest value observed in the Thrace region. Similarly, the MiHE values range approximately from −1250 to 70 nano-strain [71]. The North Aegean Sea is predominantly characterized by shear, with comparable values of MaHE and MiHE. Moreover, the MaHE and MiHE exhibit an increase in the northwestern region of Turkey, showing a slight NE–SW (MaHE orientation) extension dominance. These results indicate that the crustal dynamics of the North Aegean Trough (NAT) are more complex ranging from 100 to 700 nano-strain, particularly under a shear setting. At the same time, its extension is oriented in an NNE–SSW to N–S direction [71]. The shear occurrence can also be observed in the North Aegean Basin (NAB), characterized by moderate magnitudes and a gradual transition in an approximately

NW–SE extension direction. The NAB exhibits a prevalence of local extension dominance over compaction. The area exhibits a distinct extensional trend in contrast to the adjacent regions, which follows an ENE–WSW direction [71]. The strain regime prevalent in the northern Aegean region, except for the wider Skyros Island area, is the transition from pure to quasi-pure extension.

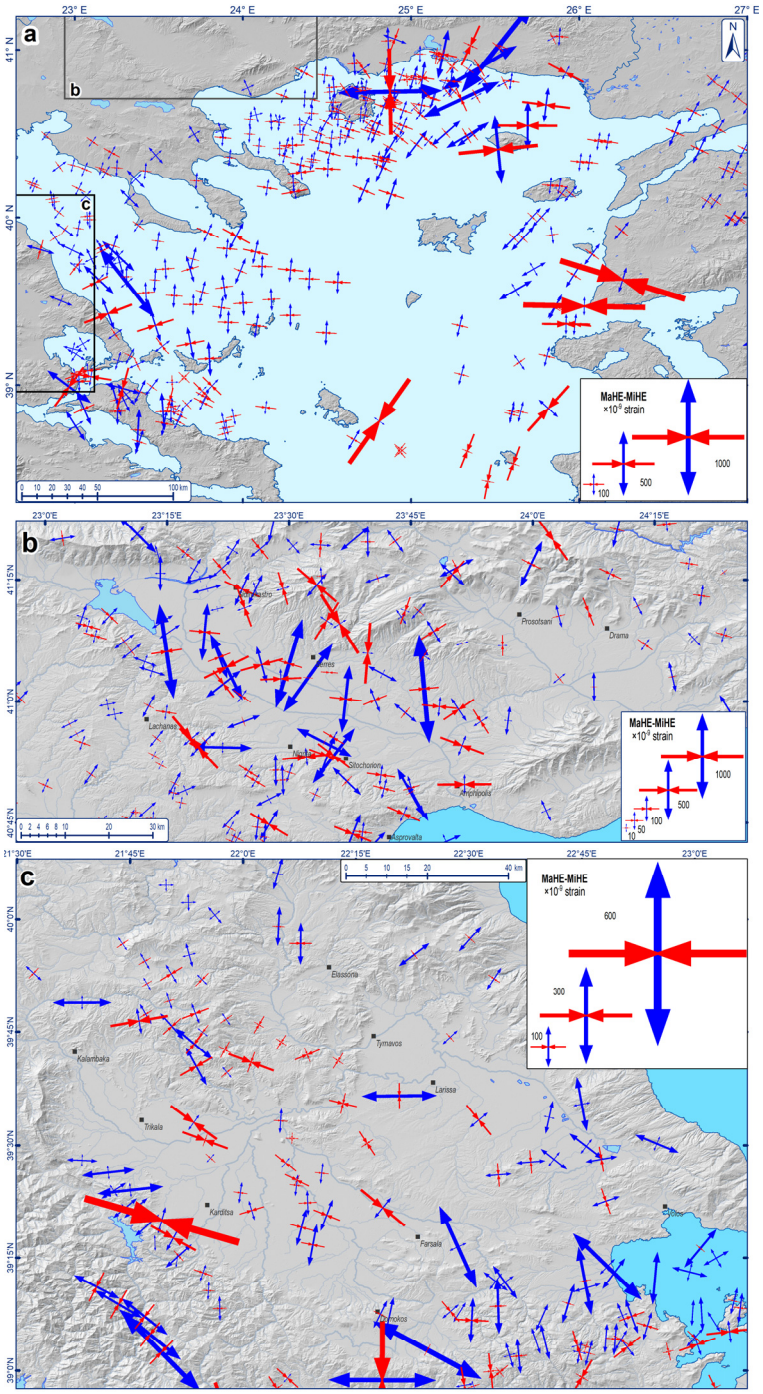

Figure 4. Maximum (MaHE; blue arrows) and Minimum (MiHE; red arrows) Horizontal Extension in the regions of: (**a**) North Aegean Sea; (**b**) Strymon basin; and (**c**) Thessalian basin.

A broad spectrum of strain field values is exhibited in the Strymon basin region. In particular, the MaHE values show a range of variability from approximately −60 to 2650×10^{-9}, whereas the corresponding MiHE values demonstrate a range of variability from approximately −650 to 150×10^{-9}, as depicted in Figure 4b. The primary analysis of

the distribution of the values [17] indicates that the absolute maximum values of both MaHE and MiHE are primarily concentrated along the eastern boundary and the northernmost part of the western boundary of the Strymon basin. Moreover, the analysis of MaHE and MiHE suggests that extension is the dominant process in the study area, resulting in a normal faulting activity. In particular, the Strymon basin exhibits a notable concentration of maximum values at its eastern and northwestern boundaries. At the same time, the high MaHE values of these regions, coupled with exceedingly low absolute values of corresponding MiHE, suggest the prevalence of dip-slip normal faulting activity [17]. The documented data reveals a gradual decrease in both MaHe and MiHE values on either side of the area. Simultaneously, the difference in values between MaHE and MiHE decreases, with MaHE values remaining greater than the corresponding MiHE values. These findings suggest oblique-slip normal faulting activity in the Strymon and the adjacent (e.g., Drama) basins. Additionally, the northwestern part of the Strymon basin exhibits positive values for both MaHE and MiHE, indicating a prevalent, pure extensional setting characterized by normal faulting. Finally, it is worth mentioning that the direction of the MaHE vectors is nearly perpendicular to the strike of the faults and fault zones, thereby providing evidence for the existence of these tectonic structures and their normal faulting characteristics.

Focusing on the wider Thessalian basin region, the values show a range of -40 to 380 nano-strain, with the extensional regime prevailing as the dominant one (Figure 2a,b) [72]. The MaHE vectors exhibit an approximate N–S orientation in the southern Thessalian basin. This region also displays the most significant values, exceeding 200 nano-strain. A notable alteration in direction is discernible towards the westernmost Thessalian basin, while similar noticeable changes are documented in the MaHE direction of the northernmost part [72]. Remarkable values exceeding 150 nano-strain are observed within the Larissa plain and the Thessalian basin southern boundary. The findings of the MaHE study indicate a progressive rise of tectonic activity in the central and eastern Thessalian basin.

4.1.2. Maximum Shear Strain (MaxSS)

The MaxSS parameter exhibits a wide distribution of values within the North Aegean Sea region, as depicted in Figure 5. These values range from 10 to 1650 nano-strain, with both peak values observed in the Samothraki Plateau. The regions that show the highest values are documented in the eastern part of the Aegean Sea (western Turkey), the CAT (Central Aegean Trough) and the NAT, as shown in Figure 5a. The MaxSS is characterized by slightly reduced values within the vicinity of the NAB, in the transitional zone that links the NAB and the CAT, and the broader region of northwestern Turkey. The regions showing great values are primarily associated with shear faulting. The extension may exhibit a greater magnitude in regions with possible oblique-to-normal dip-slip faulting. An example of such a scenario can be observed in the eastern Aegean Sea region, suggesting the occurrence of normal and oblique-slip faulting. Local kinematic variations (from pure normal dip-slip to strike-slip faulting) can be observed in regions with moderate values.

Concerning the Strymon basin, the MaxSS value analysis shows a range of approximately 1 to 2750×10^{-9} nano-strain (Figure 5a). The highest MaxSS values are recorded in the eastern region of the Strymon basin, with comparable values noted in the northwestern margin [17], respectively, as depicted in Figure 5a. Furthermore, high MaxSS values are documented in the southern region of the western boundary of the Strymon basin. The results of the geostatistical analysis, as presented in Figure 5b, provide the distribution of MaxSS. In particular, the analysis reveals that higher values of MaxSS are concentrated along the WNW–ESE axis of the Strymon basin [17]. Notably, the adjacent basins (such as the Drama basin) exhibit exceedingly low, nearly negligible values. Consequently, the significant shear values highlight the tectonic structures that are actively distributed along the boundaries of the Strymon basin, with particular emphasis on the eastern one.

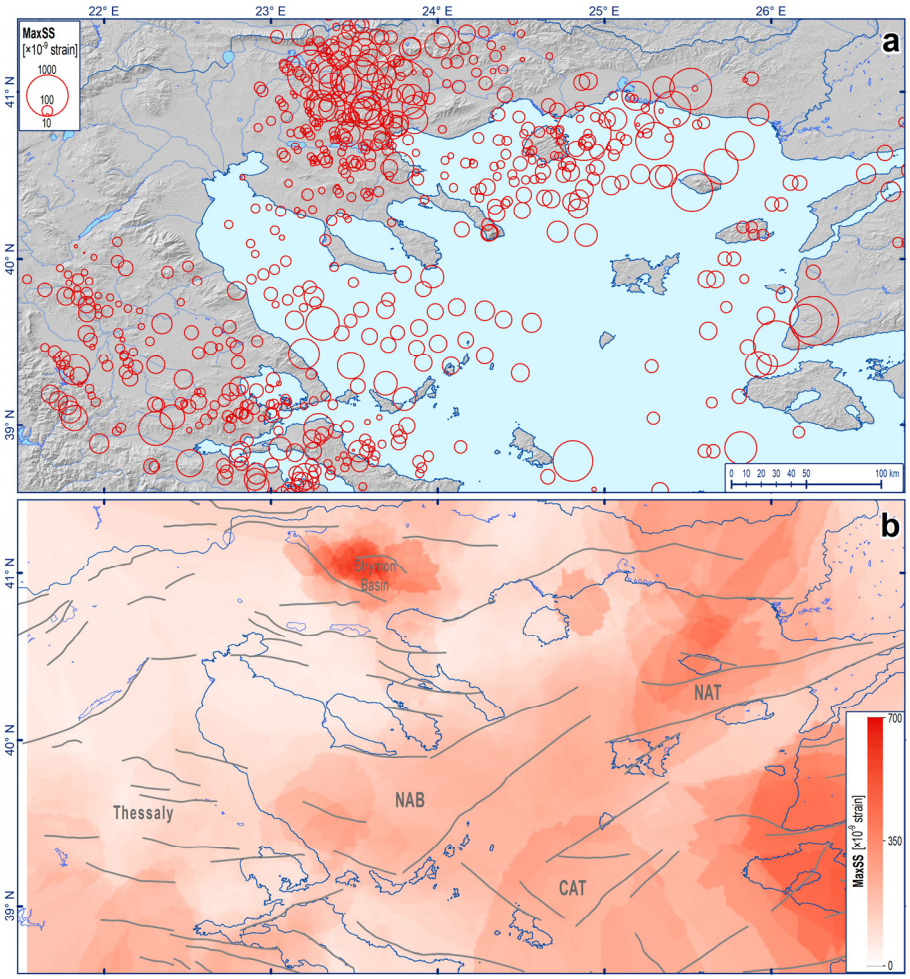

Figure 5. Maximum Shear Strain (MaxSS) in the wider North Aegean region: (**a**) MaxSS values (red circles) of all triangles, constructed within the three study areas; (**b**) MaxSS values grid, based on the interpolation (kriging) geostatistical analysis. Dark lines in (**b**) are faults (see also Figure 2).

Finally, the Thessaly area exhibits a range of MSS values from 5 to 730 nano-strain. According to the analysis of MSS values (Figure 5a,b), the regions with the highest values, exceeding 400 nano-strain, are adjacent to the western boundary of the Thessalian basin [72]; additionally, high MSS values are observed in the southern part of this region. Moreover, intermediate values (approximately 200–400 nano-strain) have been detected all along the western margin, while the northern part is characterized by low MSS values, measuring less than 100 nano-strain.

4.1.3. Area Strain (AS)

Two distinct AS types are distinguished: (i) dilatation, which is directly related to extension, and (ii) compaction, which is directly related to compression. Compaction is the predominant form of strain in the North Aegean Sea region, while the nano-strain values for AS range from −1180 (compaction) to 970 (dilatation) (Figure 6a). The dilatation encompasses a larger region (Figure 6b); the most significant values are documented in the eastern and northeastern parts of the North Aegean Sea. Samothraki Plateau and western NAB have smaller but notable dilatation values. Most compaction occurs in the southerly area of the North Aegean Sea (NAB and NAT). In particular, the CAT exhibits remarkably low values. Compaction is limited to the north of the NAB and NAT, showing a slight presence in the northeast of the North Aegean Sea and along the eastern coast of Thessaly. In a case of a vast contrast between dilatation and compaction, extensional or compressional tectonics occur, respectively. However, shear tectonics are documented in a

case of similar dilatation and compaction values. For instance, the broader NAT region is characterized by high dilatation and compaction values, defining a more complex setting, as the two strain types do not extend uniformly or equally.

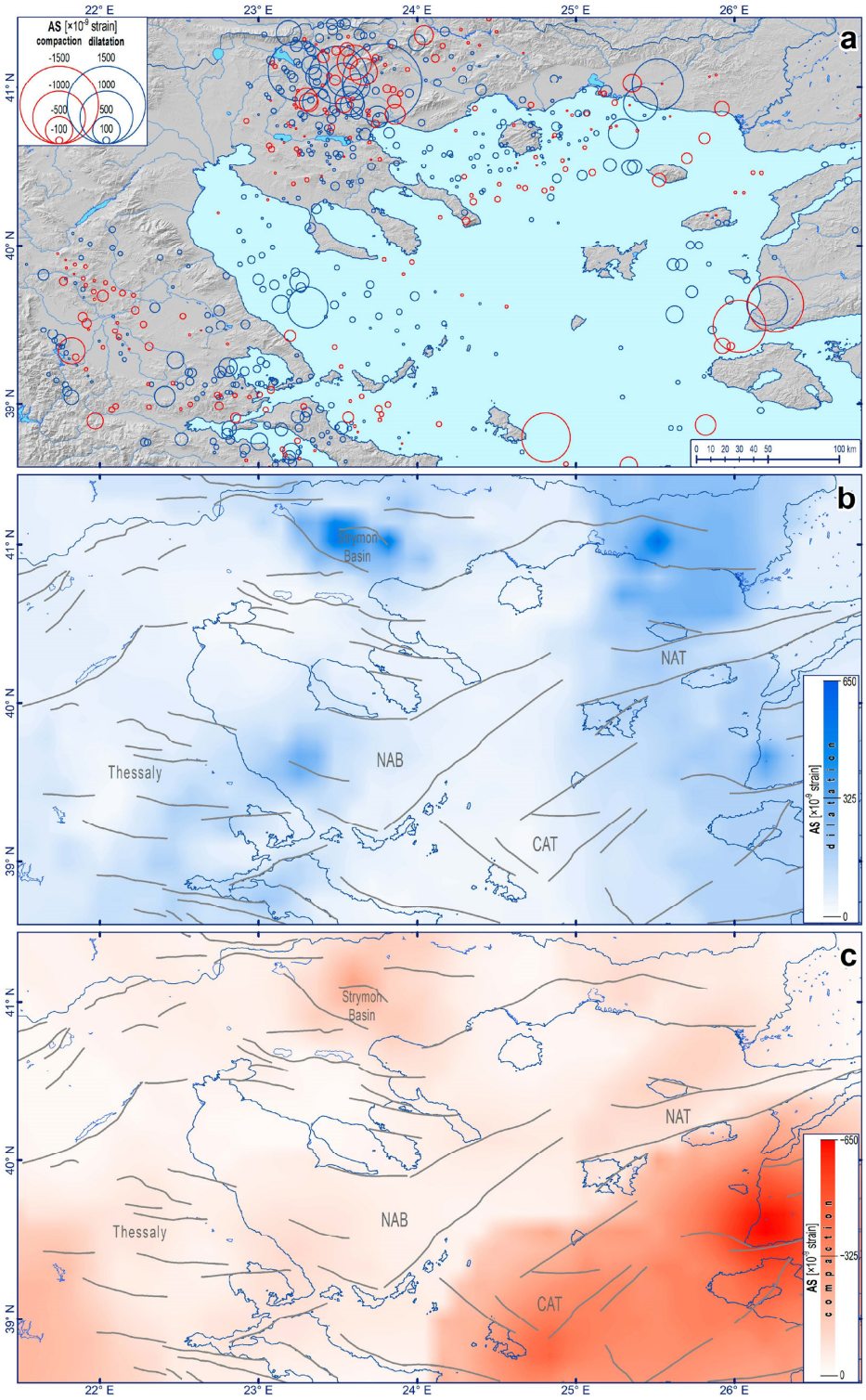

Figure 6. Area Strain (AS) in the wider North Aegean area: (**a**) Dilatation (blue circles) and compaction (red circles) calculated values; (**b**) dilatation values grid, based on the interpolation (kriging) geostatistical methodology; and (**c**) compaction values grid, based on the interpolation (kriging) geostatistical methodology. Dark lines in (**b**,**c**) are faults (see also Figure 2).

Accordingly, the AS results of the Strymon basin reveal a dilatation dominance over compaction (Figure 5a), with values ranging from approximately −600 (compaction) to 2750 × 10^{-9} (dilatation). Even though the dilatation type dominates in the Strymon basin (Figure 6b), it partially coexists with compaction, indicating shear occurrence [17]. Specifically, the greatest concentrations are only documented within the Strymon basin area, especially along the eastern margin and the northwestern part of the Strymon basin. Concerning the high-value concentrations of compaction (Figure 6b), they are predominantly documented at the eastern Strymon basin boundary [17]. The difference between dilatation and compaction defines extension (dilatation > compaction) or compression (compaction > dilatation), whereas comparable values indicate shear tectonics [71]. The Strymon basin is predominantly characterized by dilatation over compaction; nevertheless, the compaction occurrence is noteworthy, indicating that despite the dilatation dominance, a remarkable shear component is documented, leading to oblique-slip, normal faulting. A typical example is the southernmost part of the Strymon basin, which is adjacent to the North Aegean Sea and potentially affected by the corresponding strike-slip tectonic regime.

Regarding the Thessalian basin area, it exhibits AS values that vary from −420 to 360 nano-strain [72], implying occurrences of both dilatation and compaction (Figure 6a,b). The phenomenon of compaction is primarily spotted at the western boundary of Thessalian basin, where the absolute strain (AS) exceeds 100 nano-strain. However, there are also some areas in the central part, where the absolute strain ranges between 50 and 150 nano-strain. The dilatation shows a greater dispersion when higher values are considered, specifically with values exceeding 200 nano-strain in the southeastern Thessalian basin [72]; the maximum dilatation is observed to the south of the Thessalian basin. Dilatation values ranging from 100 to 200 nano-strain have been observed in the northwestern part of the Thessalian basin, while at its northern part, small values (approximately 50 nano-strain) for both compaction and dilatation are documented.

5. Discussion and Conclusions

The overall synthesis of the results gives a broader perspective on the North Aegean's geodynamic and seismotectonic setting. However, to optimise the visualisation of the combined strain parameters, we used the well-established kriging interpolation method for the MaxSS and the AS parameters, which practically reflect the MaHE and MiHE results. This method effectively distributes parameter values across the study area seamlessly, while highlighting the concentrations of extreme values and neutral-transition areas. These neutral-transition areas are important for tectonic interpretation, as they indicate transitions between different tectonic regimes.

Hence, the interpolated results highlighted new aspects in the geodynamic evolution of the study area. What strikes us the most is the intensely fast deforming area in the central part of the Strymon basin, where significant MaxSS and AS values are documented; the other area with high values is the NAT region as expected. In addition, quite high values (but distinctively lower than those above) characterize the NAB and CAT regions.

The deformation rate of the Strymon basin region exceeds the NAT is opposed to the results of other previous studies [43,45,49], according to which the NAT strain dominates in the broader northern Aegean. Although there is no doubt that the NAT is the dominant and most tectonically active structure of the broader North Aegean region, the higher values of the Strymon basin can be explained in many ways. At first, the long recording time period, i.e., seven years (2008–2014), can catch possible variations of the deformation rate; hence, during this long period, the Strymon basin might have shown more intense deformation compared to the NAT. Secondly, the seismological data suggest that seismic activity in the northern Greek mainland during the instrumentally recorded period and, especially, the very recent one could be considered as poor (Figure 2); however, few strong historic events have occurred. The NAT, as a very large, multi-segmented fault zone, exhibits frequent seismicity in all magnitudes up to approximately M_w7. Therefore, the energy is possibly released less frequently in northern Greece, waiting for the accumulated deformation and,

hence, stress to reach their highest threshold before rupturing towards a characteristic earthquake. This could also explain the long earthquake recurrence intervals in this area. From a methodological point of view, it is obvious that no barycentres have been defined within the narrow area of the NAT and the eastern part of the NAB. A denser GPS/GNSS network and, hence, denser triangles and barycentres could have shown even higher values of deformation in these particularly active areas.

Regarding the geodynamic and, in particular, the kinematics implications for the North Aegean, the MaxSS and AS syntheses indicate a transtensional regime for the Strymon basin. This area might be under the effect of the transcurrent NAT, as the CAT is to the south, forming a quasi-pull-apart basin with NW–SE-striking oblique-slip marginal faults. The NAT region shows high MaxSS values and, consequently, similarly high dilatation and compaction values (compaction slightly exceeds dilatation), implying a transpressional regime. In the NAB region, dilation becomes more dominant with much lower compaction; the MaxSS values are notable, and therefore it is concluded that the NAB undergoes E to W almost progressive transtension, shaping the trapezoidal basin with, respectively, progressively changing strike-slip to quasi-pure dip-slip normal faulting. The same pattern continues into the central Greek mainland (i.e., the Thessalian basin); however, the intensity of deformation is much lower. Finally, the coexistence of high dilatation and compaction values in the CAT region (dilatation exceeds compaction) and remarkable MaxSS values indicate transtensional strike-slip faulting.

Based on all the above, it is evident that the NAT controls the geodynamic setting of the North Aegean region. However, the geodetic analysis shed light on new geodynamic aspects in the Northern Greek mainland implying not only a fast-deforming site (Strymon basin), but a shear derived transtensional faulting, which probably extends from the Thermaikos Gulf and eastwards, reaching Thrace and western Turkey. All these shear-derived faults are potential Riedel structures strongly affected by the major NAT fault zone. This is a sensible assumption, as the CAT, located at the southern part of NAT, is also characterized by Riedel structures. Therefore, it is presumable that a similar geodynamic setting may occur in the northern part of the NAT.

Author Contributions: Conceptualization, I.L. and S.S.; methodology, I.L.; software, I.L.; validation, I.L., S.S. and C.P.; formal analysis, I.L. and C.P.; investigation, I.L. and S.S; resources, I.L., S.S. and C.P.; data curation, I.L. and S.S.; writing—original draft preparation, I.L.; writing—review and editing, I.L., S.S. and C.P.; visualization, S.S.; supervision, C.P. All authors have read and agreed to the published version of the manuscript.

Funding: This research received no external funding.

Institutional Review Board Statement: Not applicable.

Informed Consent Statement: Not applicable.

Data Availability Statement: Not applicable.

Acknowledgments: The authors would like to thank NOANET (www.gein.noa.gr (accessed on 18 April 2023)), the HxGN/SmartNet (www.metricanet.gr (accessed on 20 April 2023)), the HermesNet of AUTh (users.auth.gr/cpik (accessed on 25 April 2023)) and HEPOS (www.hepos.gr (accessed on 30 April 2023)) for providing the geodetic data.

Conflicts of Interest: The authors declare no conflict of interest.

References

1. Bevis, M. GPS Networks: The Practical Side. *Eos Trans. Am. Geophys. Union.* **1991**, *72*, 49. [CrossRef]
2. Segall, P.; Davis, J.L. GPS Applications for Geodynamics and Earthquake Studies. *Annu. Rev. Earth Planet. Sci.* **1997**, *25*, 301–336. [CrossRef]
3. McKenzie, D. Active Tectonics of the Mediterranean Region. *Geophys. J. Int.* **1972**, *30*, 109–185. [CrossRef]
4. Taymaz, T.; Jackson, J.; McKenzie, D. Active Tectonics of the North and Central Aegean Sea. *Geophys. J. Int.* **1991**, *106*, 433–490. [CrossRef]

5. Jolivet, L.; Faccenna, C.; Huet, B.; Labrousse, L.; Le Pourhiet, L.; Lacombe, O.; Lecomte, E.; Burov, E.; Denèle, Y.; Brun, J.P.; et al. Aegean Tectonics: Strain Localisation, Slab Tearing and Trench Retreat. *Tectonophysics* **2013**, *597–598*, 1–33. [CrossRef]
6. Brun, J.P.; Faccenna, C. Exhumation of High-Pressure Rocks Driven by Slab Rollback. *Earth Planet. Sci. Lett.* **2008**, *272*, 1–7. [CrossRef]
7. Philippon, M.; Brun, J.P.; Gueydan, F.; Sokoutis, D. The Interaction between Aegean Back-Arc Extension and Anatolia Escape since Middle Miocene. *Tectonophysics* **2014**, *631*, 176–188. [CrossRef]
8. Erman, C.; Yolsal-Çevikbilen, S.; Eken, T.; Tilmann, F.; Keleş, D.; Taymaz, T. Constraints on the Lithospheric Kinematics in the Aegean and Western Anatolia Unveiled by SKS Splitting Observations. *J. Geophys. Res. Solid. Earth* **2022**, *127*, e2022JB025265. [CrossRef]
9. Le Pichon, X.; Angelier, J. The Hellenic Arc and Trench System: A Key to the Neotectonic Evolution of the Eastern Mediterranean Area. *Tectonophysics* **1979**, *60*, 1–42. [CrossRef]
10. Taymaz, T.; Yilmaz, Y.; Dilek, Y. The Geodynamics of the Aegean and Anatolia: Introduction. *Geol. Soc. Spec. Publ.* **2007**, *291*, 1–16. [CrossRef]
11. Meijer, P.T.; Wortel, M.J.R. Present-Day Dynamics of the Aegean Region: A Model Analysis of the Horizontal Pattern of Stress and Deformation. *Tectonics* **1997**, *16*, 879–895. [CrossRef]
12. McKenzie, D.; Jackson, J. Conditions for Flow in the Continental Crust. *Tectonics* **2002**, *21*, 5-1–5-7. [CrossRef]
13. Sodoudi, F.; Kind, R.; Hatzfeld, D.; Priestley, K.; Hanka, W.; Wylegalla, K.; Stavrakakis, G.; Vafidis, A.; Harjes, H.P.; Bohnhoff, M. Lithospheric Structure of the Aegean Obtained from P and S Receiver Functions. *J. Geophys. Res. Solid. Earth* **2006**, *111*, B12307. [CrossRef]
14. Jolivet, L.; Menant, A.; Clerc, C.; Sternai, P.; Bellahsen, N.; Leroy, S.; Pik, R.; Stab, M.; Faccenna, C.; Gorini, C. Extensional Crustal Tectonics and Crust-Mantle Coupling, a View from the Geological Record. *Earth Sci. Rev.* **2018**, *185*, 1187–1209. [CrossRef]
15. Sboras, S.; Chatzipetros, A.; Pavlides, S. North Aegean Active Fault Pattern and the 24 May 2014, Mw 6.9 Earthquake. In *Active Global Seismology Neotectonics and Earthquake Potential. of the Eastern Mediterranean Region*; John Wiley & Sons, Inc.: Hoboken, NJ, USA, 2017; pp. 239–272. ISBN 9781118944998.
16. Reilinger, R.; McClusky, S.; Paradissis, D.; Ergintav, S.; Vernant, P. Geodetic Constraints on the Tectonic Evolution of the Aegean Region and Strain Accumulation along the Hellenic Subduction Zone. *Tectonophysics* **2010**, *488*, 22–30. [CrossRef]
17. Lazos, I.; Papanikolaou, I.; Sboras, S.; Foumelis, M.; Pikridas, C. Geodetic Upper Crust Deformation Based on Primary GNSS and INSAR Data in the Strymon Basin, Northern Greece-Correlation with Active Faults. *Appl. Sci.* **2022**, *12*, 9391. [CrossRef]
18. Brooks, M.; Ferentinos, G. Structure and Evolution of the Sporadhes Basin of the North Aegean Trough, Northern Aegean Sea. *Tectonophysics* **1980**, *68*, 15–30. [CrossRef]
19. Karakostas, V.G.; Papadimitriou, E.E.; Karakaisis, G.F.; Papazachos, C.B.; Scordilis, E.M.; Vargemezis, G.; Aidona, E. The 2001 Skyros, Northern Aegean, Greece, Earthquake Sequence: Off-Fault Aftershocks, Tectonic Implications, and Seismicity Triggering. *Geophys. Res. Lett.* **2003**, *30*, 12-1–12-14. [CrossRef]
20. Papanikolaou, D.; Nomikou, P.; Papanikolaou, I.; Lampridou, D.; Rousakis, G.; Alexandri, M. Active Tectonics and Seismic Hazard in Skyros Basin, North Aegean Sea, Greece. *Mar. Geol.* **2019**, *407*, 94–110. [CrossRef]
21. McNeill, L.C.; Mille, A.; Minshull, T.A.; Bull, J.M.; Kenyon, N.H.; Ivanov, M. Extension of the North Anatolian Fault into the North Aegean Trough: Evidence for Transtension, Strain Partitioning, and Analogues for Sea of Marmara Basin Models. *Tectonics* **2004**, *23*, TC2016. [CrossRef]
22. Papanikolaou, D.; Alexandri, M.; Nomikou, P. Active Faulting in the North Aegean Basin. *Spec. Pap. Geol. Soc. Am.* **2006**, *409*, 189–209. [CrossRef]
23. Lazos, I.; Sboras, S.; Chousianitis, K.; Kondopoulou, D.; Pikridas, C.; Bitharis, S.; Pavlides, S. Temporal Evolution of Crustal Rotation in the Aegean Region Based on Primary Geodetically-Derived Results and Palaeomagnetism. *Acta Geod. Geophys.* **2022**, *57*, 317–334. [CrossRef]
24. Robertson, A.; Dixon, J. Introduction: Aspects of the Geological Evolution of the Eastern Mediterranean. *Geol. Soc. Lond. Spec. Publ.* **1984**, *17*, 1–74. [CrossRef]
25. Mascle, J.; Martin, L. Shallow Structure and Recent Evolution of the Aegean Sea: A Synthesis Based on Continuous Reflection Profiles. *Mar. Geol.* **1990**, *94*, 271–299. [CrossRef]
26. Papanikolaou, D.J.; Royden, L.H. Disruption of the Hellenic Arc: Late Miocene Extensional Detachment Faults and Steep Pliocene-Quaternary Normal Faults-Or What Happened at Corinth? *Tectonics* **2007**, *26*, TC5003. [CrossRef]
27. Jolivet, L.; Brun, J.P. Cenozoic Geodynamic Evolution of the Aegean. *Int. J. Earth Sci.* **2010**, *99*, 109–138. [CrossRef]
28. Brun, J.P.; Sokoutis, D. Core Complex Segmentation in North Aegean, A Dynamic View. *Tectonics* **2018**, *37*, 1797–1830. [CrossRef]
29. Dewey, J.F.; Sengör, A.M.C. Aegean and Surrounding Regions. Complex Multiplate and Continuum Tectonics in a Convergent Zone. *Geol. Soc. Am. Bull.* **1979**, *90*, 84–92. [CrossRef]
30. Mercier, J.L.; Sorel, D.; Vergely, P.; Simeakis, K. Extensional Tectonic Regimes in the Aegean Basins during the Cenozoic. *Basin Res.* **1989**, *2*, 49–71. [CrossRef]
31. Koukouvelas, I.; Aydin, A. Fault Structure and Related Basins of the North Aegean Sea and Its Surroundings. *Tectonics* **2002**, *21*, 10-1–10-17. [CrossRef]
32. Sternai, P.; Jolivet, L.; Menant, A.; Gerya, T. Driving the Upper Plate Surface Deformation by Slab Rollback and Mantle Flow. *Earth Planet. Sci. Lett.* **2014**, *405*, 110–118. [CrossRef]

33. Bocchini, G.M.; Brüstle, A.; Becker, D.; Meier, T.; van Keken, P.E.; Ruscic, M.; Papadopoulos, G.A.; Rische, M.; Friederich, W. Tearing, Segmentation, and Backstepping of Subduction in the Aegean: New Insights from Seismicity. *Tectonophysics* **2018**, *734–735*, 96–118. [CrossRef]
34. Lybéris, N. Tectonic Evolution of the North Aegean Trough. *Geol. Soc. Lond. Spec. Publ.* **1984**, *17*, 709–725. [CrossRef]
35. Dinter, D.A.; Royden, L. Late Cenozoic Extension in Northeastern Greece: Strymon Valley Detachment System and Rhodope Metamorphic Core Complex. *Geology* **1993**, *21*, 45–48. [CrossRef]
36. Pavlides, S.; Kilias, A. Neotectonic and Active Faults along the Serbomacedonian Zone (SE Chalkidiki, Northern Greece). *Ann. Tecton.* **1987**, *1*, 97–104.
37. Mountrakis, D.; Tranos, M.; Papazachos, C.; Thomaidou, E.; Karagianni, E.; Vamvakaris, D. Neotectonic and Seismological Data Concerning Major Active Faults, and the Stress Regimes of Northern Greece. *Geol. Soc. Spec. Publ.* **2006**, *260*, 649–670. [CrossRef]
38. Cerrone, C.; Di Donato, V.; Mazzoli, S.; Robustelli, G.; Soligo, M.; Tuccimei, P.; Ascione, A. Development and Deformation of Marine Terraces: Constraints to the Evolution of the Campania Plain Quaternary Coastal Basin (Italy). *Geomorphology* **2021**, *385*, 107725. [CrossRef]
39. Sboras, S. *The Greek Database of Seismogenic Sources: Seismotectonic Implications for North Greece*; University of Ferrara: Ferrara, Italy, 2011.
40. Caputo, R.; Chatzipetros, A.; Pavlides, S.; Sboras, S. The Greek Database of Seismogenic Sources (GreDaSS): State-of-the-Art for Northern Greece. *Ann. Geophys.* **2012**, *55*, 859–894. [CrossRef]
41. Noomen, R.; Springer, T.A.; Ambrosius, B.A.C.; Herzberger, K.; Kuijper, D.C.; Mets, G.-J.; Overgaauw, B.; Wakker, K.F. Crustal Deformations in the Mediterranean Area Computed from SLR and GPS Observations. *J. Geodyn.* **1996**, *21*, 73–96. [CrossRef]
42. Becker, M. Assessment of Height Variations by GPS at Mediterranean and Black Sea Coast Tide Gauges from the SELF Projects. *Glob. Planet. Change* **2002**, *34*, 5–35. [CrossRef]
43. Pérouse, E.; Chamot-Rooke, N.; Rabaute, A.; Briole, P.; Jouanne, F.; Georgiev, I.; Dimitrov, D. Bridging Onshore and Offshore Present-Day Kinematics of Central and Eastern Mediterranean: Implications for Crustal Dynamics and Mantle Flow. *Geochem. Geophys. Geosyst.* **2012**, *13*, Q09013. [CrossRef]
44. Müller, M.D.; Geiger, A.; Kahle, H.G.; Veis, G.; Billiris, H.; Paradissis, D.; Felekis, S. Velocity and Deformation Fields in the North Aegean Domain, Greece, and Implications for Fault Kinematics, Derived from GPS Data 1993–2009. *Tectonophysics* **2013**, *597–598*, 34–49. [CrossRef]
45. Serpelloni, E.; Faccenna, C.; Spada, G.; Dong, D.; Williams, S.D.P. Vertical GPS Ground Motion Rates in the Euro-Mediterranean Region: New Evidence of Velocity Gradients at Different Spatial Scales along the Nubia-Eurasia Plate Boundary. *J. Geophys. Res. Solid. Earth* **2013**, *118*, 6003–6024. [CrossRef]
46. Jenny, S.; Goes, S.; Giardini, D.; Kahle, H.G. Earthquake Recurrence Parameters from Seismic and Geodetic Strain Rates in the Eastern Mediterranean. *Geophys. J. Int.* **2004**, *157*, 1331–1347. [CrossRef]
47. Kahle, H.G.; Straub, C.; Reilinger, R.; McClusky, S.; King, R.; Hurst, K.; Veis, G.; Kastens, K.; Cross, P. The Strain Rate Field in the Eastern Mediterranean Region, Estimated by Repeated GPS Measurements. *Tectonophysics* **1998**, *294*, 237–252. [CrossRef]
48. Billiris, H.; Paradissis, D.; Veis, G.; England, P.; Featherstone, W.; Parsons, B.; Cross, P.; Rands, P.; Rayson, M.; Sellers, P.; et al. Geodetic Determination of Tectonic Deformation in Central Greece from 1900 to 1988. *Nature* **1991**, *350*, 124–129. [CrossRef]
49. Clarke, P.J.; Davies, R.R.; England, P.C.; Parsons, B.; Billiris, H.; Paradissis, D.; Veis, G.; Cross, P.A.; Denys, P.H.; Ashkenazi, V.; et al. Crustal Strain in Central Greece from Repeated GPS Measurements in the Interval 1989–1997. *Geophys. J. Int.* **1998**, *135*, 195–214. [CrossRef]
50. Chousianitis, K.; Ganas, A.; Evangelidis, C.P. Strain and Rotation Rate Patterns of Mainland Greece from Continuous GPS Data and Comparison between Seismic and Geodetic Moment Release. *J. Geophys. Res. Solid. Earth* **2015**, *120*, 3909–3931. [CrossRef]
51. England, P.; Houseman, G.; Nocquet, J.-M. Constraints from GPS Measurements on the Dynamics of Deformation in Anatolia and the Aegean. *J. Geophys. Res. Solid. Earth* **2016**, *121*, 8888–8916. [CrossRef]
52. D'Agostino, N.; Métois, M.; Koci, R.; Duni, L.; Kuka, N.; Ganas, A.; Georgiev, I.; Jouanne, F.; Kaludjerovic, N.; Kandić, R. Active Crustal Deformation and Rotations in the Southwestern Balkans from Continuous GPS Measurements. *Earth Planet. Sci. Lett.* **2020**, *539*, 116246. [CrossRef]
53. Caporali, A.; Aichhorn, C.; Barlik, M.; Becker, M.; Fejes, I.; Gerhatova, L.; Ghitau, D.; Grenerczy, G.; Hefty, J.; Krauss, S.; et al. Surface Kinematics in the Alpine-Carpathian-Dinaric and Balkan Region Inferred from a New Multi-Network GPS Combination Solution. *Tectonophysics* **2009**, *474*, 295–321. [CrossRef]
54. Le Pichon, X.; Chamot-Rooke, N.; Lallemant, S.; Noomen, R.; Veis, G. Geodetic Determination of the Kinematics of Central Greece with Respect to Europe: Implications for Eastern Mediterranean Tectonics. *J. Geophys. Res.* **1995**, *100*, 12675–12690. [CrossRef]
55. McClusky, S.; Balassanian, S.; Barka, A.; Demir, C.; Ergintav, S.; Georgiev, I.; Gurkan, O.; Hamburger, M.; Hurst, K.; Kahle, H.; et al. Global Positioning System Constraints on Plate Kinematics and Dynamics in the Eastern Mediterranean and Caucasus. *J. Geophys. Res.* **2000**, *105*, 5695. [CrossRef]
56. Kahle, H.G.; Cocard, M.; Peter, Y.; Geiger, A.; Reilinger, R.; Barka, A.; Veis, G. GPS-Derived Strain Rate Field within the Boundary Zones of the Eurasian, African, and Arabian Plates. *J. Geophys. Res. Solid. Earth* **2000**, *105*, 23353–23370. [CrossRef]
57. Nyst, M.; Thatcher, W. New Constraints on the Active Tectonic Deformation of the Aegean. *J. Geophys. Res. B Solid. Earth* **2004**, *109*, 1–23. [CrossRef]
58. Nocquet, J.M. Present-Day Kinematics of the Mediterranean: A Comprehensive Overview of GPS Results. *Tectonophysics* **2012**, *579*, 220–242. [CrossRef]

59. Simpson, R.W.; Thatcher, W.; Savage, J.C. Using Cluster Analysis to Organize and Explore Regional GPS Velocities. *Geophys. Res. Lett.* **2012**, *39*, L18307. [CrossRef]
60. Avallone, A.; Briole, P.; Agatza-Balodimou, A.M.; Billiris, H.; Charade, O.; Mitsakaki, C.; Nercessian, A.; Papazissi, K.; Paradissis, D.; Veis, G. Analysis of Eleven Years of Deformation Measured by GPS in the Corinth Rift Laboratory Area. *Comptes Rendus Geosci.* **2004**, *336*, 301–311. [CrossRef]
61. Floyd, M.A.; Billiris, H.; Paradissis, D.; Veis, G.; Avallone, A.; Briole, P.; McClusky, S.; Nocquet, J.-M.; Palamartchouk, K.; Parsons, B.; et al. A New Velocity Field for Greece: Implications for the Kinematics and Dynamics of the Aegean. *J. Geophys. Res.* **2010**, *115*, B10403. [CrossRef]
62. Cocard, M.; Kahle, H.G.; Peter, Y.; Geiger, A.; Veis, G.; Felekis, S.; Paradissis, D.; Billiris, H. New Constraints on the Rapid Crustal Motion of the Aegean Region: Recent Results Inferred from GPS Measurements (1993-1998) across the West Hellenic Arc, Greece. *Earth Planet. Sci. Lett.* **1999**, *172*, 39–47. [CrossRef]
63. Briole, P.; Rigo, A.; Lyon-Caen, H.; Ruegg, J.C.; Papazissi, K.; Mitsakaki, C.; Balodimou, A.; Veis, G.; Hatzfeld, D.; Deschamps, A. Active Deformation of the Corinth Rift, Greece: Results from Repeated Global Positioning System Surveys between 1990 and 1995. *J. Geophys. Res. Solid. Earth* **2000**, *105*, 25605–25625. [CrossRef]
64. Lagios, E.; Sakkas, V.; Papadimitriou, P.; Parcharidis, I.; Damiata, B.N.; Chousianitis, K.; Vassilopoulou, S. Crustal Deformation in the Central Ionian Islands (Greece): Results from DGPS and DInSAR Analyses (1995–2006). *Tectonophysics* **2007**, *444*, 119–145. [CrossRef]
65. Hollenstein, C.; Müller, M.D.; Geiger, A.; Kahle, H.G. Crustal Motion and Deformation in Greece from a Decade of GPS Measurements, 1993-2003. *Tectonophysics* **2008**, *449*, 17–40. [CrossRef]
66. Reilinger, R.; McClusky, S.; Vernant, P.; Lawrence, S.; Ergintav, S.; Cakmak, R.; Ozener, H.; Kadirov, F.; Guliev, I.; Stepanyan, R.; et al. GPS Constraints on Continental Deformation in the Africa-Arabia-Eurasia Continental Collision Zone and Implications for the Dynamics of Plate Interactions. *J. Geophys. Res. Solid. Earth* **2006**, *111*, B05411. [CrossRef]
67. Vernant, P.; Reilinger, R.; McClusky, S. Geodetic Evidence for Low Coupling on the Hellenic Subduction Plate Interface. *Earth Planet. Sci. Lett.* **2014**, *385*, 122–129. [CrossRef]
68. Faccenna, C.; Bellier, O.; Martinod, J.; Piromallo, C.; Regard, V. Slab Detachment beneath Eastern Anatolia: A Possible Cause for the Formation of the North Anatolian Fault. *Earth Planet. Sci. Lett.* **2006**, *242*, 85–97. [CrossRef]
69. Reilinger, R.; McClusky, S. Nubia-Arabia-Eurasia Plate Motions and the Dynamics of Mediterranean and Middle East Tectonics. *Geophys. J. Int.* **2011**, *186*, 971–979. [CrossRef]
70. Mantovani, E.; Babbucci, D.; Tamburelli, C.; Viti, M. Late Cenozoic Evolution and Present Tectonic Setting of the Aegean–Hellenic Arc. *Geosciences* **2022**, *12*, 104. [CrossRef]
71. Lazos, I.; Sboras, S.; Pikridas, C.; Pavlides, S.; Chatzipetros, A. Geodetic Analysis of the Tectonic Crustal Deformation Pattern in the North Aegean Sea, Greece. *Mediterr. Geosci. Rev.* **2021**, *3*, 79–94. [CrossRef]
72. Lazos, I.; Sboras, S.; Chousianitis, K.; Bitharis, S.; Mouzakiotis, E.; Karastathis, V.; Pikridas, C.; Fotiou, A.; Galanakis, D. Crustal Deformation Analysis of Thessaly (Central Greece) before the March 2021 Earthquake Sequence near Elassona-Tyrnavos (Northern Thessaly). *Acta Geodyn. Geomater.* **2021**, *18*, 379–385. [CrossRef]
73. Bitharis, S.; Fotiou, A.; Pikridas, C.; Rossikopoulos, D. A New Velocity Field of Greece Based on Seven Years (2008–2014) Continuously Operating GPS Station Data. In *Earth and Environmental Sciences for Future Generations*; Springer: Cham, Switzerland, 2016; pp. 321–329.
74. Fotiou, A.; Rossikopoulos, D.; Katsougiannopoulos, S.; Tsioukas, V.; Pikridas, C.; Spatalas, S. The Hermes GNSS NtripCaster of AUTh. *Bull. Geod. Geophys.* **2009**, *69*, 35–43.
75. Boehm, J.; Werl, B.; Schuh, H. Troposphere Mapping Functions for GPS and Very Long Baseline Interferometry from European Centre for Medium-Range Weather Forecasts Operational Analysis Data. *J. Geophys. Res. Solid. Earth* **2006**, *111*, B02406. [CrossRef]
76. Herring, T.A.; King, R.W.; Floyd, M.A.; Mcclusky, S.C. GAMIT Reference Manual. GPS Analysis at MIT 2015. Massachusetts Institute of Technology, MA, USA. Available online: http://geoweb.mit.edu/gg/docs/GAMIT_Ref.pdf (accessed on 10 January 2023).
77. Bitharis, S. Study of the Geodynamic Field in Greece Using Modern Satellite Geodetic Methods. Ph.D. Thesis, School of Rural and Surveying Engineering, Aristotle University of Thessaloniki, Thessaloniki, Greece, 2021.
78. Hashimoto, M.; Jackson, D.D. Plate Tectonics and Crustal Deformation around the Japanese Islands. *J. Geophys. Res.* **1993**, *98*, 16149. [CrossRef]
79. Shen, Z.K.; Jackson, D.D.; Ge, B.X. Crustal Deformation across and beyond the Los Angeles Basin from Geodetic Measurements. *J. Geophys. Res. B Solid. Earth* **1996**, *101*, 27957–27980. [CrossRef]
80. Sagiya, T.; Nishimura, T.; Iio, Y.; Tada, T. Crustal Deformation around the Northern and Central Itoigawa-Shizuoka Tectonic Line. *Earth Planets Space* **2002**, *54*, 1059–1063. [CrossRef]
81. Lazos, I.; Pikridas, C.; Chatzipetros, A.; Pavlides, S. Determination of Local Active Tectonics Regime in Central and Northern Greece, Using Primary Geodetic Data. *Appl. Geomat.* **2020**, *13*, 3–17. [CrossRef]
82. Arnoso, J.; Riccardi, U.; Benavent, M.; Tammaro, U.; Montesinos, F.G.; Blanco-Montenegro, I.; Vélez, E. Strain Pattern and Kinematics of the Canary Islands from GNSS Time Series Analysis. *Remote. Sens.* **2020**, *12*, 3297. [CrossRef]
83. Lyros, E.; Kostelecky, J.; Plicka, V.; Vratislav, F.; Sokos, E.; Nikolakopoulos, K. Detection of Tectonic and Crustal Deformation Using GNSS Data Processing: The Case of PPGnet. *Civ. Eng. J.* **2021**, *7*, 14–23. [CrossRef]

84. Lazos, I.; Stergiou, C.L.; Chatzipetros, A.; Pikridas, C.; Bitharis, S.; Melfos, V. Active Tectonics (Extensional Regime and Rotations) and Tertiary Mineralization Occurrences within Central Macedonia, Greece. In Proceedings of the 9th International INQUA Meeting on Paleoseismology, Active Tectonics and Archeoseismology (PATA), Possidi, Greece, 25–27 June 2018; pp. 145–148.
85. Available online: http://www.unavco.org (accessed on 14 February 2023).